Effect of synthesis methods on the physico-chemical and catalytic properties of Ni 13X and Ni 5A zeolite catalysts in CO_2 methanation

Wei, Liangyuan; Kumar, Narendra; Haije, Wim; Peltonen, Janne; Peurla, Markus; Grénman, Henrik; de Jong, Wiebren

DOI
10.1016/j.cattod.2025.115239

Publication date
2025

Document Version
Final published version

Published in
Catalysis Today

Catalysis Today 452 (2025) 115239

Contents lists available at ScienceDirect

Catalysis Today

journal homepage: www.elsevier.com/locate/cattod

Effect of synthesis methods on the physico-chemical and catalytic properties of Ni 13X and Ni 5A zeolite catalysts in CO_2 methanation

Liangyuan Wei [a], Narendra Kumar [b], Wim Haije [c], Janne Peltonen [d], Markus Peurla [e], Henrik Grénman [b,*], Wiebren de Jong [a,*]

[a] Faculty ME, Department of Process and Energy, Section Large-Scale Energy Storage, Delft University of Technology, Delft, the Netherlands
[b] Faculty of Science and Engineering, Johan Gadolin Process Chemistry Centre, Laboratory of Industrial Chemistry and Reaction Engineering, Åbo Akademi University, Turku/Åbo, Finland
[c] Faculty of Applied Sciences, Materials for Energy Conversion and Storage, Delft University of Technology, Delft, the Netherlands
[d] Department of Physics and Astronomy, University of Turku, Turku, Finland
[e] Institute of Biomedicine, University of Turku, Finland

ARTICLE INFO

Keywords:
Synthesis methods
Ni
13X and 5A zeolite catalysts
CO_2 methanation

ABSTRACT

Zeolite 13X and 5A were modified with nickel using three different methods: evaporation impregnation, deposition precipitation, and ion-exchange for comparison in CO_2 methanation. The catalysts were tested in a lab scale fixed bed reactor and their physico-chemical properties were characterized by XRD, SEM-EDX, TEM, STEM-EDX, nitrogen physisorption, H_2-TPR and NH_3-TPD. The physico-chemical characterization results of Ni modified 13X and 5A zeolite catalysts showed that the zeolite structure did not change after the Ni modification by different catalyst synthesis methods, although the surface area and micro-pore volume decreased. The average diameter of NiO and the NiO cluster size range of Ni zeolite catalyst synthesized with ion exchange are smaller than the catalysts prepared by the evaporation impregnation and deposition preparation. Ni dispersed well through 13X, while a lot of Ni appeared on the crystal outer surface of 5A zeolite. Evaporation impregnation and deposition precipitation prepared Ni13X catalysts exhibited a higher activity than ion-exchange prepared samples on CO_2 methanation. The catalyst performance of Ni5A-IE and Ni13X-IE zeolite catalysts, which were synthesized using the ion-exchange method for CO_2 methanation was limited by the actual loading of Ni. The Ni 13X catalysts have less CH_4 selectivity which could be attributed to their lower acidity. Ni13X-EIM catalyst showed good catalytic stability at 360 °C, with no catalyst deactivation during a 200 h catalyst stability test.

1. Introduction

Carbon dioxide is one of the most important greenhouse gases; capturing and reducing the emission of CO_2 have gained much attention [1,2]. Converting CO_2 into sustainable energy carriers is one of the important methods for countering global warming and energy issues, which humanity is facing today [3,4]. On the other hand, more and more wind and solar power plants are being built in order to produce more renewable and environmentally friendly electricity [5]. However, large scale electricity storage is a key issue for the efficient utilization of these renewable energy source, due to the intermittent nature of wind and solar sources as well as the energy demand fluctuations [3]. The methanation of carbon dioxide with renewable H_2 is a promising way to store energy at a large scale this is then based on Sabatier reaction: $CO_2 + 4\ H_2 \leftrightarrow CH_4 + 2\ H_2O$; $\Delta H^0_{298} = -165$ kJ/mol [6,7]. CO_2 methanation also plays a vital role in the upgrading of the product gas after biomass gasification or pyrolysis [8,9].

A high purity of the substitute gas is required by the gas grid [10]. Sorption enhanced methanation is an efficient way to remove water close to the catalytically active sites and shift the Sabatier reaction equilibrium towards the products according to LeChatelier's principle for obtaining high conversion [10,11]. The main challenge is to balance the sorption enhancement and catalytic performance of the (bifunctional) catalysts in CO_2 methanation. The (bifunctional) catalysts should have high activity at low temperatures where thermodynamics are favorable, high selectivity towards CH_4, high stability as well as high

* Corresponding authors.
E-mail addresses: l.wei@tue.nl (L. Wei), Narendra.Kumar@abo.fi (N. Kumar), whaije@cs.com (W. Haije), janne.pltonen@utu.fi (J. Peltonen), markus.peurla@utu.fi (M. Peurla), henrik.grenman@abo.fi (H. Grénman), Wiebren.deJong@tudelft.nl (W. de Jong).

https://doi.org/10.1016/j.cattod.2025.115239
Received 31 October 2024; Received in revised form 10 January 2025; Accepted 13 February 2025
Available online 19 February 2025

water uptake capacity. By using a physical mixture of commercial Ni catalyst and zeolite 4 A at 250, 350 °C, Walspurger et al. obtained pure CH_4 from the sorption enhanced Sabatier reaction [10]. Using a bifunctional catalyst which combines the Ni catalytic function and the sorption effect of zeolite could be an elegant and efficient method in process development [12,13]. Delmelle et al. found that Ni on zeolite 5 A and 13X catalysts have a high activity and CH_4 selectivity in the sorption enhanced CO_2 methanation [14]. Wei et al. found that Ni 13X always has higher activity than Ni 5 A for CO_2 methanation [15,16]. Some other zeolites, such as Zeolite USY [17,18] and HNaUSY [19], were chosen as the catalysts supports by some researchers due to their high crystallinity, uniform porosity, and resistance to catalyst deactivation. Because of high activity, CH_4 selectivity and cost, Ni based catalysts are the most widely used catalysts for CO_2 methanation [20,21]. By comparison, Ni 13X catalyst has shown the highest performance among these catalysts; the CO_2 conversion values were lower than 20 % at 350 °C (GHSV=43000h^{-1}) for other Ni USY catalysts [14,17–19].

Thus, zeolite supported catalysts are advantageous for CO_2 methanation, especially for producing high purity of substitute natural gas. However, most CO_2 methanation publications have focused on new catalysts with different metals on conventional supports, such as Al_2O_3 [22] and SiO_2 [23], and those catalysts were mainly prepared by impregnation, while the studies on different catalyst synthesis methods were limited [7,24–26]. In general, the catalyst activity will be influenced by different preparation methods, since the active metal dispersion, cluster size, and location (inside or outside the cages, pores, and channels) [19], the acidity, part of the Si-Al framework, or extra framework will be different. The pH of the solution for catalyst preparation using the deposition-precipitation method was varied using NH_4OH aqueous solution, which would influence the catalyst property; ion-exchange could lead to highly dispersed catalyst. The pH change and washing procedures are the main differences among evaporation impregnation, deposition precipitation and ion-exchange.

The current work focuses on the synthesis of Ni- modified 13X and 5 A zeolite catalysts using three different methods and physico-chemical characterizations using various techniques. Moreover, the catalytic activity and selectivity of the Ni 13X and Ni 5 A zeolite catalysts were investigated in CO_2 methanation with the aim of correlating the properties of the catalysts with the obtained performance. However, to compare the catalytic properties of Ni zeolite catalysts prepared by different methodologies, the current work mainly focuses on catalytic CO_2 methanation without water sorption enhancement. In this paper, Ni13X-EIM, Ni13X-DP and Ni13X-IE, Ni5A-EIM, Ni5A-DP, and Ni5A-IE catalysts were prepared by evaporation impregnation (EIM), deposition precipitation (DP) and ion-exchange (IE), respectively. The pH of the solution was monitored with a pH meter during catalyst preparation. After the catalyst were prepared, XRD, SEM-EDX, TEM, STEM-EDX, nitrogen physisorption, H_2-TPR were used to characterize them for their crystal structure, morphology, NiO cluster size, surface area, and pore volume. Additionally, NH_3-TPD was used to determine the acidic properties of catalysts. The activity and selectivity tests of the catalysts were carried out in a lab scale fixed bed reactor system [27].

2. Experiments

2.1. Catalyst preparation

Zeolite 13X and 5A were modified with nickel using three different methods: evaporation impregnation, deposition precipitation, and ion-exchange. In the ion-exchange process, a solution was prepared with a soluble salt of the desired loading of cations (nickel ions) in water, the zeolite was added into the solution for ion-exchange in hours, then the aqueous solution was separated away from the zeolite by filtration [28,29]. For the deposition precipitation process, the zeolite was put into the nickel precursor solution and the solution was thoroughly stirred, then the precipitating agent was added gradually. After a given time, the solid sample was washed and dried [30]. In the evaporation impregnation method, the zeolite was put into the nickel precursor solution, and the solution was rotated for a given time, then the aqueous solution was evaporated in the rotating evaporator [28]. The evaporation impregnation method did not involve any washing step [28].

The catalyst Ni13X-EIM and Ni5A-EIM were prepared by the evaporation impregnation method (EIM). As it was expected that a good dispersion is obtained and a high porosity of the support is maintained for our sorption enhanced CO_2 methanation study [13], a Ni- metal loading of 5 wt% was targeted. Nickel nitrate hexahydrate ($Ni(NO_3)_2$•6 H_2O, 99 %, Merck Millipore) was used as the Ni precursor. The Ni precursor was dissolved in 250 mL of distilled water in a flask, and 5 g of 0.212–0.500 mm size sieve fraction (dried at 100 °C overnight in an oven) 13X or 5 A zeolite (Merck Millipore, The Netherlands) was added to the solution. A pH meter was used to measure the pH of the solution during the process. The rotating evaporator was operated at a low rotation speed of 10 rpm, for 24 h at room temperature. After 24 h of catalyst synthesis, evaporation of the aqueous solution was carried out in the rotating evaporator at 50 °C using a water jet pump. The obtained solid sample was dried at 100 °C before calcination.

In the catalysts (Ni5A-DP and Ni13X-DP) preparation by deposition precipitation (DP), nickel nitrate hexahydrate ($Ni(NO_3)_2$•6 H_2O, 99 %, Merck Millipore) was dissolved in 250 mL distilled water in a beaker, and the solution was stirred with a low stirring speed, after which 5 g of dry 5 A or 13X zeolite was added to the solution. Ammonium hydroxide solution (25 wt%, for analysis, Merck KGaA) was used to increase the pH of the solution from neutral to around 9.6 after several minutes, and stirring was continued for 24 h before washing the catalyst with around 1 L of distilled water, then the sample was left at room temperature overnight, after which it was moved to an oven for drying overnight at 100 °C before calcination.

Ion-exchange(IE) was also used as a method in the catalyst preparation (Ni13X-IE and Ni5A-IE) [29]. The nickel nitrate salt solution was prepared like above, and 5 g of dry 13X or 5 A zeolite was added into the solution. The pH of the solution was monitored by a pH meter during the preparation, and the mixture solution was stirred around 24 h before filtering and washing with at least 1 L distilled water, after which the obtained solid sample was dried at 100 °C in an oven overnight before calcination.

All catalysts were calcined in a muffle furnace using a step calcination procedure. In the stepwise procedure, the heating rate from room temperature to 250 °C was 4.5 °C/min, and then temperature was kept for 40 min; after which the temperature was increased to the target temperature 400 °C by 2.5 °C/min, where it was kept for 3 h and then cooled down to room temperature. The calcination program was designed for obtaining a highly active catalyst with small Ni clusters [31]. Increasing temperature from room temperature to 250 ℃ with 4.5 ℃/min was performed to remove H_2O and to get $Ni_3(NO_3)_2(OH)_4$, after which a lower temperature increase of 2.5 ℃/min to 400 ℃ was used, aiming at nickel oxide formation from $Ni_3(NO_3)_2(OH)_4$. The mass loss then was around 40 % when temperature was increased from 260 to 380 ℃ [32]. It was found that Ni zeolite catalyst calcined at 400 ℃ had a better performance in CO_2 methanation compared to higher or lower temperatures, as presented in our previous publication [15].

2.2. Catalyst characterization

The calcined catalysts (before reduction) were characterized by X-ray powder diffraction (XRD), scanning electron microscopy (SEM), transmission electron microscopy (TEM), scanning transmission electron microscopy equipped with energy-dispersive X-ray spectroscopy (STEM-EDX), nitrogen physisorption, hydrogen temperature programed reduction (H_2-TPR), and temperature programmed ammonia desorption (NH_3-TPD).

The PANalytical Empyrean X-ray powder diffractometer was used in the XRD measurements. The diffractometer was operated in Bragg-

Brentano diffraction mode, and the monochromatized Cu-Kα radiation (λ = 1.541874 Å) was generated with a voltage of 45 kV and a current of 40 mA. The measured XRD diffractograms were analyzed with Philips X'Pert HighScore (phase analysis refinement) and MAUD programs (background subtraction), and the scanning 2θ angle range was 3.0° to 80.0 step size 0.013°, using a counting time of 80 seconds/step.

Catalysts morphology, shape, size and distributions of crystals were studied by scanning electron microscopy (SEM) LEO Gemini 1530 (LEO/ZEISS, Germany). The catalysts' elemental analysis was carried out by energy dispersive X-ray spectroscopy (EDX).

Transmission electron microscopy (TEM) was used to study the Ni-cluster size and distributions. The average NiO cluster size was then calculated. Furthermore, structure and morphology were also investigated using transmission electron microscopy. The equipment used was JEM-1400 (JEOL Itd, Japan) with a maximum acceleration voltage is 120 kV.

To further study the nanoscale of the catalysts synthesized, scanning transmission electron microscopy equipped with an energy-dispersive X-ray spectroscopy (STEM-EDX) detector was used. The equipment used was FEI Titan 80–300 electron microscope, the elemental mapping was investigated at a voltage of 300 kV with EDX. Specimen preparation consisted of immersing a lacey carbon film supported on a copper grid into the catalysts powder, small clusters adhering to the carbon film were measured.

The surface area, pore size, and pore volume of pristine 13X and 5 A zeolite, Ni- modified 13X and 5 A zeolite catalysts were measured using nitrogen physisorption method. The instrument used was Sorptomatic 1900 (Carlo Erba Instruments). The calculation of surface area was carried out using Dubinin method. The catalysts were outgassed at 350 °C for 3 h prior to the surface area measurement.

H_2-TPR analysis was carried out in a Micromeritics AutoChem 2910. Catalysts were dried at 250 °C for 1 h in a dry Ar atmosphere, then reduced by 5 % H_2 (diluted by Ar) from room temperature to 900 °C with 5 °C/min heating rate, a TCD detector was used to monitor the H_2 consumption.

Temperature programmed desorption was carried out using a Micromeritics AutoChem 2910 to investigate the acidity of the catalysts, and samples were dried at 250 °C for 0.5 h with dry He before ammonia adsorption (5 % NH_3 diluted by He). The desorption temperatures ranged from 100 to 900 °C.

2.3. Catalysts test

The prepared catalysts' activity, selectivity, and stability were characterized in a quartz fixed-bed reactor system described in our previous work [27].

In the catalyst test, 0.9 g of catalyst was loaded into the reactor and reduced under 100 mL/min H_2 atmosphere at 500 °C for 4 hours. The reduction temperature was selected based on the results obtained in our previous study [15]. Catalysts' activity tests were performed from 240 °C to 440 °C with a gas hourly space velocity (GHSV) of 13333 mL/g cat/h. In the Sabatier reaction, 40 mL/min H_2 and 10 mL/min CO_2 diluted by N_2 (150 mL/min) were introduced. The product gas from the reactor was led through a cooling condenser and dryer, then analyzed by GC (Varian, CP-4900 Micro-GC).

The CO_2 conversion (1) and catalyst selectivity (2) for CH_4 are defined as [15,26]:

$$X_{CO_2} = \frac{n_{CO_{2,in}} - n_{CO_{2,out}}}{n_{CO_{2,in}}} \quad (1)$$

$$S_{CH_4} = \frac{n_{CH_{4,out}}}{n_{CO_{2,in}} - n_{CO_{2,out}}} \quad (2)$$

Where n_{CO_2} is the input molar flow rate of CO_2 in the experiment, $n_{CO_{2,out}}$ and $n_{CH_{4,out}}$ are the molar flow rate of CO_2 and CH_4 calculated from GC results, respectively (selectivity <100 % means that CO is formed).

The CO_2 equilibrium conversion was calculated based on the gas-phase equilibrium constant equation [33]. The equilibrium constant for each temperature can be found in literature or a database e.g. FactSage.

3. Results and discussion

3.1. Catalyst structure and surface properties

3.1.1. X-ray powder diffraction (XRD)

The XRD background corrected diffractograms for Ni- 13X and 5 A zeolite catalysts prepared with different methods, fresh 13X and 5 A zeolites are shown in Fig. 1. The XRD patterns indicated that the evaporation impregnation, deposition precipitation, and ion-exchange methods for the catalyst preparation did not change the 13X and 5 A zeolite crystal structure. Additionally, most of the peaks for NiO were not obvious in the XRD spectrum, except for the weak peaks at the position of around 2θ= 43° for Ni5A-DP and Ni5A-EIM catalysts (right, Fig. 1). The plausible explanation for this observation could be the low amount of NiO present in the Ni- 13X and 5 A zeolite catalysts which resulted in weak peaks, and their peaks overlapped with or were too close to zeolites' crystal at the positions such as 2θ= 37°, 43°, 63°, 75° and 79° [34].

3.1.2. Scanning electron microscopy (SEM) and Energy dispersive X-ray spectroscopy (EDX)

SEM was used to investigate the morphology of Ni zeolite catalysts, as shown in Fig. S. 1 (supplementary material). The 5 A zeolite showed around 2 μm porous crystals, the fresh 5 A zeolite showed the smoothest crystal surface compared to the catalysts prepared using evaporation impregnation, deposition precipitation and ion exchange. The honeycomb type architecture on the 5 A zeolite crystal surface could be NiO crystals, which were visible only on the Ni modified 5 A zeolite surface. However, it is difficult to find any differences between the Ni modified 13X zeolite catalysts and the fresh 13X zeolite, which indicates that the fibrous morphology of 13X zeolite did not change after the Ni modification using different preparation methods.

SEM combined with EDX was employed to investigate the morphology and chemical composition of Ni- 5 A and Ni- 13X catalysts, which were synthesized by different methods. It was observed that the ratio of Al to Si in 13X and 5 A zeolite did not change after modification, while Na concentration decreased after Ni modification by deposition precipitation and ion-exchange (Table S. 2, supplementary material). The actual loading of Ni is different for catalysts prepared by various methods, which is 3.2 %, 3.5 %, 1.4 %, 3.9 %, 2.9 %, and 1.7 % (mass percentages) for catalyst Ni13X-EIM, Ni13X-DP, Ni13X-IE, Ni5A-EIM, Ni5A-DP, and Ni5A-IE, respectively. The lowest loading of Ni was rather expectedly obtained using the ion-exchange (IE) method, since Na^+ is the most likely exchangeable ion in 13X and 5A with Ni, and Na is located in 13X and 5A zeolite cages, which makes it difficult to exchange with Ni [35]. Moreover, some un-exchanged Ni ions were washed out in catalyst preparation via ion-exchange. However, for the evaporation impregnation method, the increased nickel nitrate hexahydrate concentration resulted from the water evaporation which was rather beneficial as more Ni ions were facilitated to enter into the zeolite structure. More than two times higher concentrations of Ni were determined in the catalysts prepared by evaporation impregnation and deposition precipitation methods compared to the ion-exchange method. Therefore, for Ni modified 13X and 5A zeolite catalysts, it can be concluded that a higher Ni loading can be easier obtained by evaporation impregnation and deposition precipitation, in comparison to ion-exchange.

3.1.3. Transmission electron microscopy (TEM)

The NiO cluster size, distribution and morphology were investigated

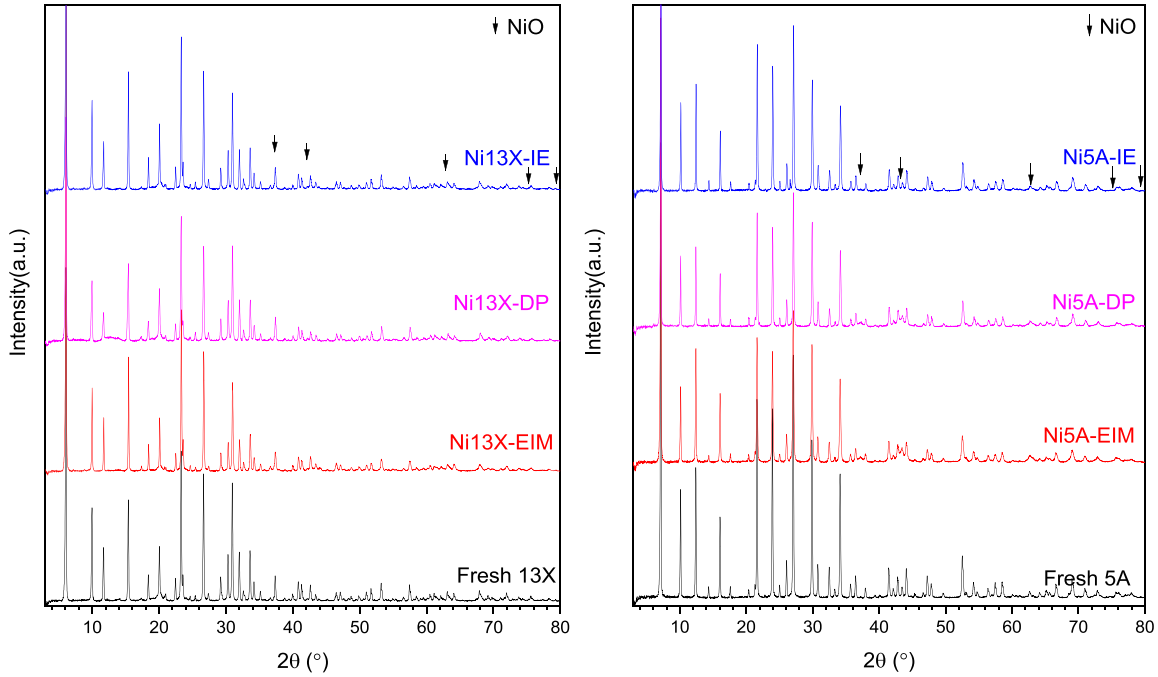

Fig. 1. The XRD background corrected diffractograms for Ni 13X(left) and 5 A(right) zeolite catalysts with different preparation methods, fresh 13X and 5 A zeolite.

using transmission electron microscopy (TEM), as shown in Fig. 2. It is noticeable that a small NiO cluster size of around 10 nm can be obtained with all three methods: evaporation impregnation, deposition precipitation and ion-exchange (Table S. 3, supplementary material). Meanwhile, one should keep the idea in mind that the NiO cluster size calculation in this section was based on the visible clusters. However, the visually observed value of the cluster size distribution does not exclude the presence of smaller clusters inside the pores of the zeolite. The smallest average NiO cluster size was obtained for catalysts prepared by ion-exchange (Table S. 3, supplementary material), which is around 7.4 nm for Ni5A-IE. Deposition precipitation can also lead to an average cluster size around 9.6 nm, which is very close to 9.7 nm obtained from the evaporation impregnation method for Ni 5 A catalysts. However, the NiO cluster size is around 12.3 nm and 42.7 nm for Ni 13X catalysts obtained from evaporation impregnation and deposition precipitation, respectively.

However, the NiO cluster size range is from 4.3 to 13.1 nm for the catalyst Ni5A-IE prepared by ion-exchange, which is the smallest. Meanwhile, the Ni13X-IE catalyst also has a limited NiO cluster size range. It can be concluded, that the catalyst synthesis methods have a significant effect on the NiO cluster size distribution when loading Ni on 13X and 5 A zeolite. The ion-exchange resulted in a narrow cluster size distribution for Ni- modified 13X and 5 A zeolite.

3.1.4. *STEM-EDX*

TEM is useful to illustrate the NiO dispersion. However, TEM pictures show the NiO dispersion on a thin layer of catalysts without element information. Thus, it is not perfect to show the NiO dispersion on 13X and 5A zeolite big crystal by TEM. In fact, the NiO dispersion is influenced by the property of the zeolite, e.g. the pore size and crystal size of zeolite. Moreover, some very small nano NiO clusters would be invisible in TEM pictures, while these metal sites are always associated with high activity in reaction because of their high surface free energy [27,36]. Therefore, elemental mapping was carried out on STEM-EDX to further investigate the dispersion of the NiO cluster in catalysts.

Because Na^{+} and Ca^{2+} the zeolites can be exchangeable with Ni^{2+} during catalysts synthesis, the concentration profiles were studied with STEM.EDX and are depicted in Fig. 3. Moreover, most other elements have concentrations less than 10 wt% (Table S. 2, supplementary material). The STEM images, Na (gold), Ca (blue), and Ni (red) maps of Ni-zeolite catalysts with different methods of preparations are shown in Fig. 3. It can be seen that Ni dispersed well through 13X zeolite for Ni13X-EIM, Ni13X-DP, Ni13X-IE. However, in contrast, Ni dispersion was not good on 5 A zeolite for the catalysts prepared by evaporation impregnation, deposition precipitation or ion-exchange, Ni appeared like an egg shell coating on 5 A zeolite.

Therefore, it can be concluded that most Ni dispersed on the crystal surface of 5 A zeolite using evaporation impregnation, deposition precipitation and ion-exchange. This is very different to the Ni dispersion through 13X zeolite catalysts prepared by the three different methods.

3.1.5. *Nitrogen physisorption*

Nitrogen physisorption was used to determine the specific surface area and pore volume of 13X, 5 A zeolite, Ni-13X and Ni-5A zeolite catalysts; the results are shown in Table S. 4 (supplementary material).

Fresh 13X zeolite has the highest surface area with a value of 655 m^2/g, which is followed by Ni13X-IE (595 m^2/g) and fresh 5A zeolite (593 m^2/g). These Ni catalysts have lower micropore volume than fresh 13X and 5A zeolite. The most plausible reason for the decrease in surface area and micropore volume is the blocking of micropores with small NiO clusters during catalyst calcination. Some small NiO clusters expectedly block the zeolite pores inside the zeolite, while larger clusters may block the pores of the zeolites from the outer surface of the support. The catalyst Ni13X-EIM prepared by evaporation impregnation exhibited the lowest surface area (361 m^2/g), attributed to the blocking of micropores with NiO clusters. The ion-exchange method exhibited the highest surface area (595 m^2/g) among the Ni modified catalysts, which can be attributed to lower loading and smaller nanoclusters of NiO (8.85 nm; see supplementary material Table S. 3) on 13X and 5 A zeolites.

3.1.6. *H_2-Temperature programmed reduction (TPR)*

The H_2-Temperature programed reduction (H_2-TPR) profiles are shown in Fig. 4 for fresh 13X zeolite, Ni13X-EIM, Ni13X-DP, Ni13X-IE, fresh 5 A zeolite, Ni5A-EIM, Ni5A-DP and Ni5A-IE.

As can be seen from Fig. 4 (left), one strong peak is present at around

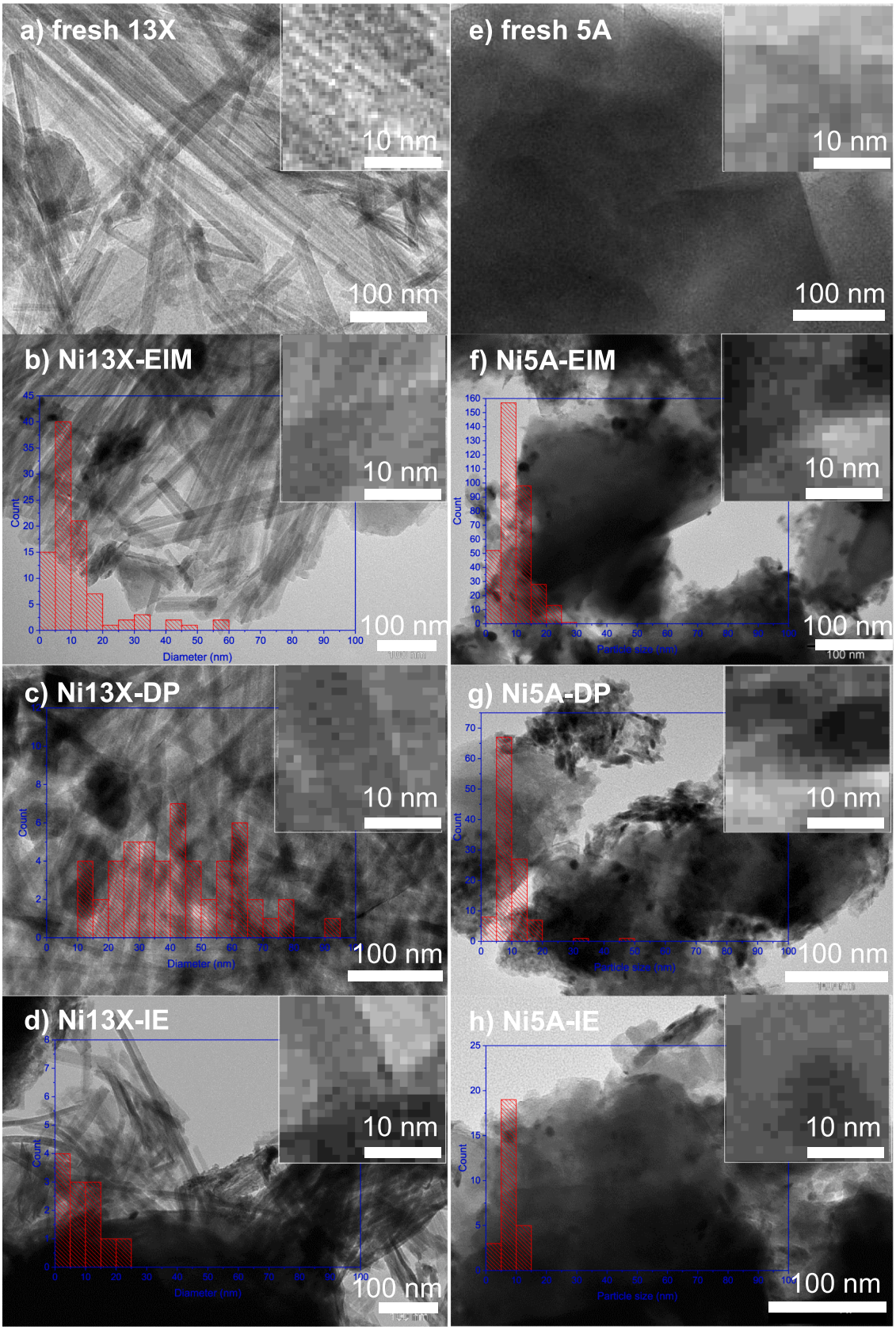

Fig. 2. TEM images of a) fresh 13X, b) Ni13X-EIM, c) Ni13X-DP, d) Ni13X-IE, e) fresh 5 A, f) Ni5A-EIM, g) Ni5A-DP and h) Ni5A-IE.

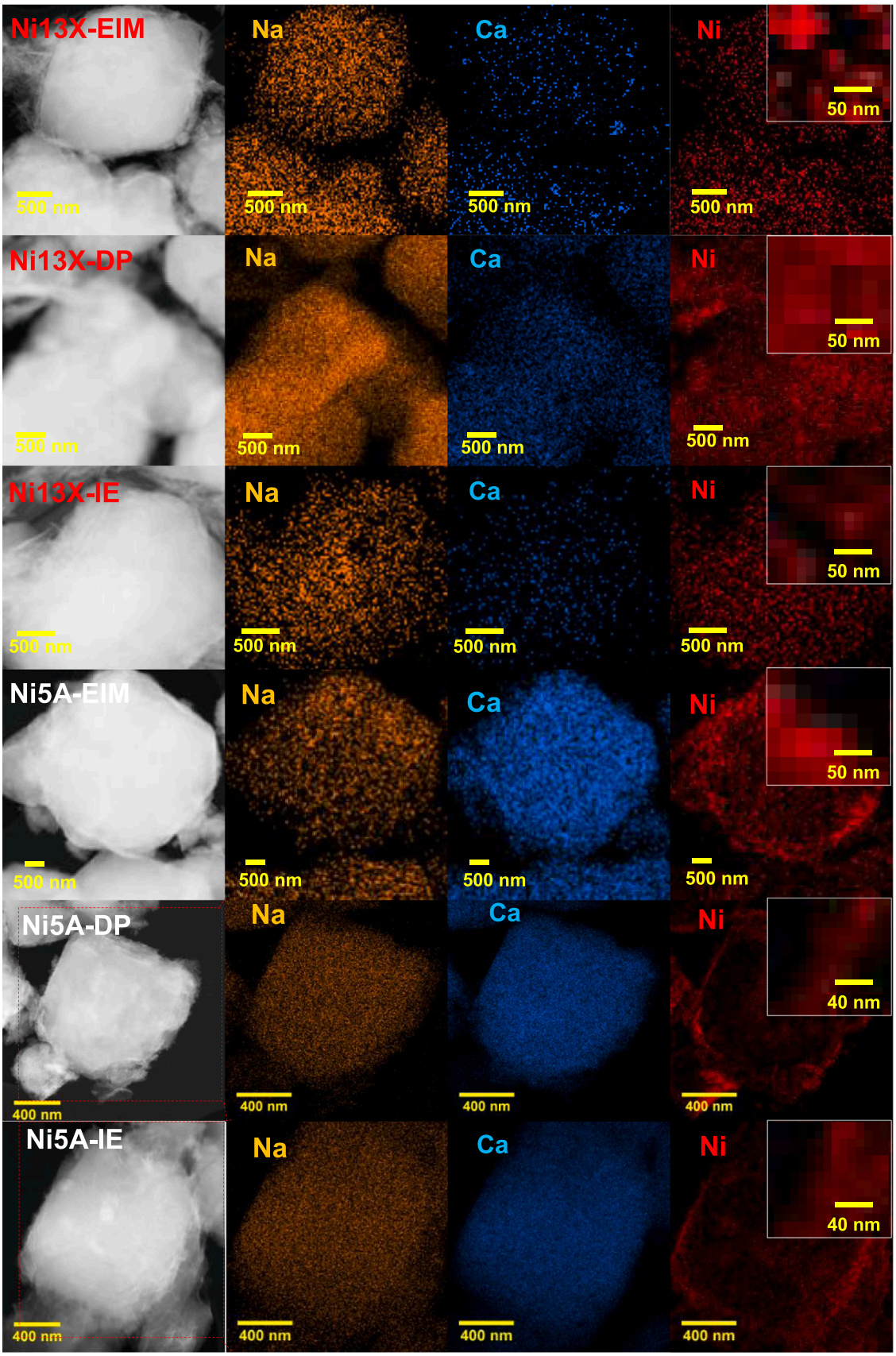

Fig. 3. STEM images (first row), Na (gold), Ca (light blue) and Ni (red) maps of Ni13X-EIM, Ni13X-DP, Ni13X-IE, Ni5A-EIM, Ni5A-DP and Ni5A-IE.

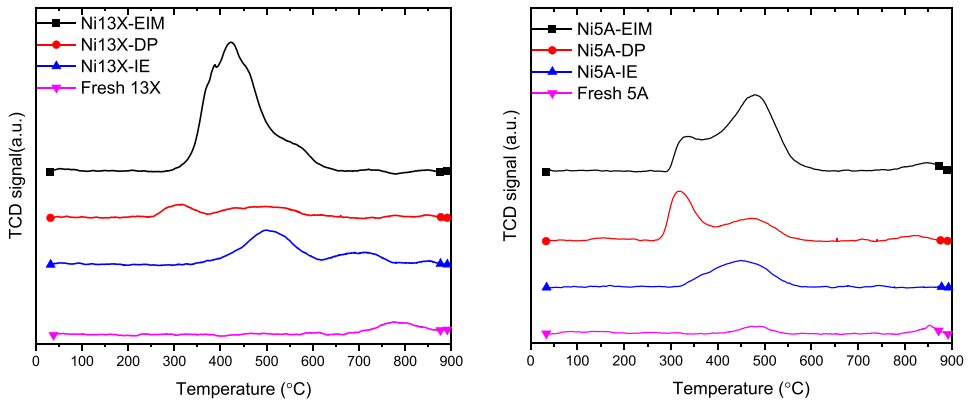

Fig. 4. H_2-TPR profiles of Ni13X-EIM, Ni13X-DP, Ni13X-IE, fresh 13X zeolite, Ni5A-EIM, Ni5A-DP, Ni5A-IE and fresh 5 A zeolite.

420 °C for the catalyst Ni13X-EIM prepared by evaporation impregnation, while the peak comes out at around 300 °C for the catalyst prepared by deposition precipitation, and it is not very clear like the one from Ni13X-EIM. However, the peaks for Ni13X-IE are positioned around 500 °C and 700 °C. These temperatures are higher than the catalysts prepared by evaporation impregnation and deposition precipitation methods. This may be because the NiO clusters are difficult to be reduced since they are located in the super cages and sodalite cages of 13X zeolite, respectively [19,26]. On the contrary, more NiO clusters stay at the surface of 13X zeolite after calcination and were easy to be reduced. This may be related to the nickel hydroxoaqua complexes generated in the solution during catalysts preparation [37–39], and the pore size of 13X zeolite limited the possibility of NiO to enter into the super cages and sodalite cages.

As is shown in Fig. 4 (right), one peak can be found at around 480 °C for all of Ni-5A catalysts. There exists only this single peak for catalyst Ni5A-IE prepared by ion-exchange, while there is another peak at around 325 °C for both catalysts Ni5A-EIM and Ni5A-DP, which were prepared by evaporation impregnation and deposition precipitation methods, respectively. This may result from those NiO clusters in the Ni5A-IE catalyst which are difficult to be reduced since they are located in the super cages of 5A zeolite [19,26]. While, more NiO clusters stayed at the surface of 5A zeolite after calcination and were easy to be reduced. This may related to the nickel hydroxoaqua complexes generated in solution during catalysts preparation [37–39], and the possibility of Ni enter into the super cages of 5A zeolite was limited due to the pore size of 5A zeolite. The H_2-TPR results provided important information of catalyst reduction prior to using them in experiments. Combining our previous study on Ni zeolite catalyst [15], the catalysts reduction under 100 mL/min H_2 atmosphere at 500 °C for 4 hours were performed in this work. These reduction conditions were expected to reduce most NiO clusters in/on zeolite to metallic Ni^0 [40].

3.1.7. *Temperature programmed desorption of ammonia (NH_3-TPD)*

NH_3-TPD was used to investigate the acidic properties of 13X, 5 A zeolites and Ni modified catalysts which were synthesized using different methods.

It was found that Ni13X-EIM has the lowest weak acidity, and this was followed by Ni13X-DP (Fig. 5). The total acidity decreased for Ni 13X catalysts prepared using different methods compared to fresh 13X, while it did not change much for Ni 5 A catalysts. The pore blocking of the Ni clusters could be one possible reason for the decrease in acidity of catalysts [41]. In this respect, also Ni13X-EIM has the lowest surface area, see Table S. 4 (supplementary material). The substantial decrease in the total acid sites of Ni 13X zeolite is attributed to the substitution of acid sites by NiO nanoclusters. For fresh 13X zeolite and Ni13X-DP, a peak at around 175 °C and a peak at around 625 °C can be found (Fig. S. 2, supplementary material), which correspond to the weak (175 °C) and

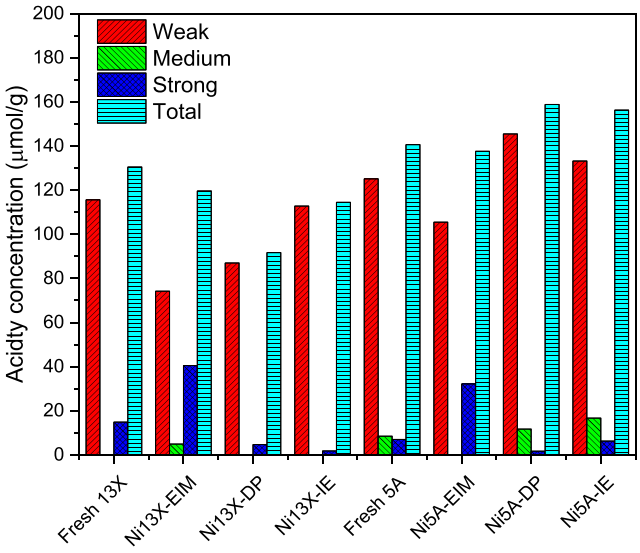

Fig. 5. The catalyst acidity distribution calculated based on the results of NH_3-TPD.

strong (625 °C) acid sites, respectively [42–44]. However, a shoulder appeared at around 250 °C for catalysts Ni13X-EIM and Ni13X-IE. For fresh 5 A zeolite, a wide peak at around 100–400 °C can be observed, and the NH_3-TPD profiles of Ni- modified catalysts Ni5A-EIM, Ni5A-DP, and Ni5A-IE are similar to 5 A zeolite. In fact, the peaks at 200 °C and 300 °C consist of several narrow peaks, which could correspond to different acid sites [42,43].

It can be concluded that evaporation impregnation, deposition-precipitation, and ion-exchange lead to the change of Ni 13X and Ni 5 A zeolite catalysts weak, medium, strong and total acid sites distributions, especially on Ni 13X catalysts. These changes in different types of acid sites are attributed to the substitutions of acid sites by NiO nanoclusters. The ion-exchange method has less influence on catalyst acidity, while evaporation impregnation is conducive to getting a lower weak acidity and strong acidity. Plausible explanations for the decrease in acid sites can be attributed to higher loadings of Ni on the surface and inside the structures of 13X and 5A zeolites using evaporation impregnation and deposition precipitation methods. The amount of Ni loadings synthesized in Ni 13X and Ni 5A zeolites using ion-exchange method is lower than evaporation impregnation and deposition precipitations.

3.2. Evaluation of catalytic properties for CO_2 methanation in a fixed bed reactor

3.2.1. Catalyst activity and selectivity

The catalyst activity and selectivity tests were carried out in the lab scale fixed bed quartz reactor system described before [27]. As the adsorption catalyst was already saturated with water before activity and selectivity data were collected, adsorption enhancement can be excluded from the data. The CO_2 conversion and CH_4 selectivity curves for the catalysts Ni13X-EIM, Ni13X-DP, Ni13X-IE, Ni5A-EIM, Ni5A-DP and Ni5A-IE, are shown in Fig. 6. Most of the CO_2 conversion curves show a similar trend, which increases systematically from lower than 10 % to equilibrium values. The highest conversion was obtained at 360 °C to 450 °C, and it is different for different catalysts. This is due to thermodynamic limitations when temperature was increased [14,45]. The catalyst performance was compared to results from literature [14, 15,17,19,22,46,47], and this is presented in Table 1. The CO_2 conversion rate for the Ni13X-EIM catalyst in the current work reached 0.00656 mol_CO_2/mol_Ni/s at 280 °C, which was in the higher level range compared to other Ni zeolite catalysts [14,15]. Considering that the particle size of zeolite 13X was much larger than in reference [22], and the CO_2 methanation mechanism might be different for different supports, the Ni zeolite catalysts in this work were promising for CO_2 methanation.

The catalysts Ni13X-DP and Ni13X-EIM Ni5A-EIM displayed the highest activity, followed by Ni5A-EIM. Considering the high GHSV, the result is very good. The lowest CO_2 conversion was obtained from the catalyst Ni5A-IE (Fig. 6), which is lower than the conversion obtained from Ni13X-IE and Ni5A-DP catalysts. This could be resulting from the limited actual loading of Ni on 13X and 5A zeolite for the catalysts prepared by ion exchange (Table S.2, supplementary material), which leads to less active sites. However, the Ni dispersion was not good for Ni5A-DP (Fig. 2). Additionally, for the Ni13X-IE and Ni5A-IE catalysts most of the NiO was located in super cages and sodalite cages of 13X and 5A zeolite according to the results of H_2-TPR (Fig. 4). This may affect the performance of Ni5A-IE and Ni13X-IE on CO_2 methanation as well. By contrast, Ni-13X catalysts have a higher activity than Ni-5A catalysts prepared using three different methods, which would be due to the dispersion of Ni being better through 13X zeolite than 5A (Fig. 2). Considering that the Ni13X-EIM and Ni13X-DP presented lower surface area and pore volume (Table S. 1, supplementary material) compared to fresh zeolite 13X, some small Ni clusters would dispersed in the zeolite 13X pores and channels.

It can be seen that the catalysts Ni5A-EIM, Ni5A-DP and Ni5A-IE display a high CH_4 selectivity, most of them higher than 90 % at temperatures lower than 400 °C. That is because the Sabatier reaction is exothermic, and CO production via the reverse water gas shift reaction (RWGS) is thermodynamically favored at high temperature [16,55]. By contrast, the CH_4 selectivity is much lower for Ni13X-EIM, Ni13X-DP, Ni13X-IE at low temperature, this could be the reason that Ni 13X catalysts have less acidity sites than Ni 5A catalysts (Fig. 5). Overall, a weak acidity of Ni zeolite 13X or 5A catalyst was favorable for a higher activity [16,27], while this might result in a lower CH_4 selectivity. Besides, according to the results obtained in our previous study, the basicity of Ni zeolite catalysts should not be too strong to avoid too strong bonding of CO_2 [27], which would be kept in mind during Ni zeolite catalyst synthesis for CO_2 methanation.

3.2.2. Catalyst stability and selectivity

After the activity test of the catalysts, a stability test of Ni13X-EIM was carried out at 360 °C for 200 hours. The catalyst was reduced at 500 °C for 4 hours before the stability test. The CO_2 conversion and CH_4 selectivity trends are shown in Fig. 7. It can be observed that Ni13X-EIM displayed a very stable performance and no indications of deactivation could be observed during the 200 hours test at 360 ℃. At the same time, a stable CH_4 selectivity of 97 % was obtained from Ni13X at 200 hours stability test. It can be seen that the stability of Ni13X-EIM is very good compared to literature results [14,15,17,19,22,46,47] (Table 1).

4. Conclusions

Ni modified 13X and 5 A zeolite catalysts were synthesized using evaporation impregnation, deposition precipitation and ion-exchange methods. The physico-chemical properties of the pristine 13X, 5 A zeolite and Ni- modified 13X, 5A zeolite catalysts were characterized using XRD, SEM-EDX, TEM, STEM-EDX, N_2 physisorption and TPD-NH_3.

It was observed that the methods of catalyst synthesis influenced the formation of NiO cluster size and the amounts of weak medium and strong acid sites. Furthermore, Ni- contents, surface area and pore volume were observed to be influenced by the methods of catalyst synthesis. The surface area, micropore volume decreased after the Ni modification of 13X and 5A zeolite due to pore blockage with large NiO nanoclusters. A smaller NiO cluster size was obtained for NiO modified catalysts using ion exchange method. A lot of Ni appeared on the surface of 5A crystals, while Ni appeared more homogeneous through 13X. The catalyst preparation methods such as evaporation impregnation, deposition precipitation and ion-exchange were observed to influence the catalytic activity in CO_2 methanation. The catalyst Ni13X-EIM exhibited stable performance on activity and CH_4 selectivity during a 200 hours' test. Therefore, evaporation impregnation method is promising for Ni

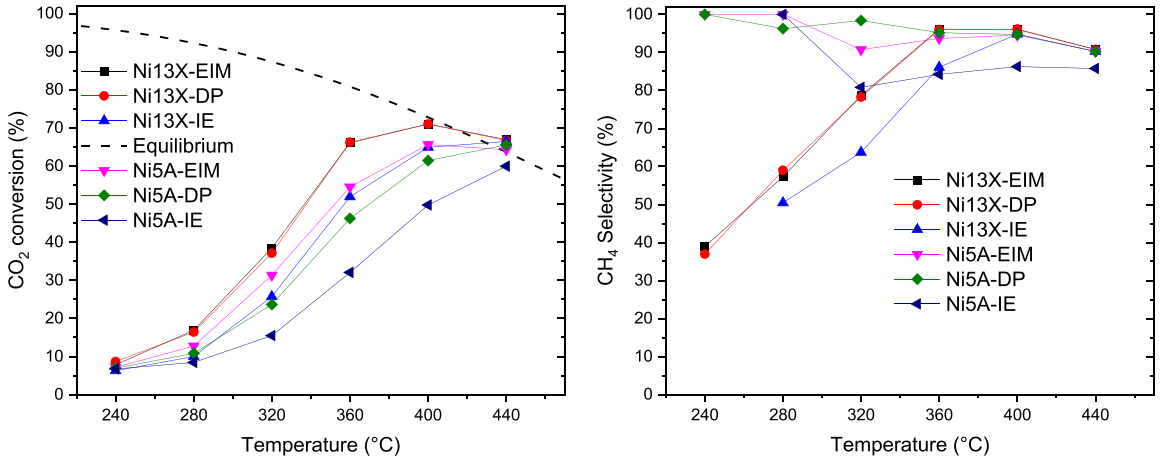

Fig. 6. CO_2 conversion and CH_4 selectivity with catalyst Ni13X-EIM, Ni13X-DP, Ni13X-IE, Ni5A-EIM, Ni5A-DP and Ni5A-IE (0.9 g, reduction at 500 °C, 4 h), 150 mL/min N_2, 40 mL/min H_2, 10 mL/min CO_2.

Table 1
Catalysts performance comparison with results from open literature, most experiments carried out at 1 bar except reference [48] at 5 bar.

Catalyst[a]	Met.[b]	Size_C[c] (nm)	Size_P[d] (mm)	$m_{Cat.}$ (g)	H_2/CO_2/ Inert gas ratio	Stab.[e] (h)	GHSV Or WHSV	CO_2 Conversion (%) T (°C)	CH_4 Selectivity (%) T (°C)	Rate (mol_CO_2/ mol_Ni/s)[f]	Ref.
Ni13X-EIM	EIM	12.3	0.212–0.5	0.9	4:1:15	200	13333 mL/g/h	16.9, 280	57.3, 280	0.00656	This work
Ni13X-DP	DP	42.7	0.212–0.5	0.9	4:1:15	-	13333 mL/g/h	16.4, 280	59.0, 280	0.00637	This work
Ni13X-IE	IE	8.8	0.212–0.5	0.9	4:1:15	-	13333 mL/g/h	10.0, 280	50.4, 280	0.00388	This work
Ni5A-EIM	EIM	9.7	0.212–0.5	0.9	4:1:15	-	13333 mL/g/h	12.8, 280	100, 280	0.00497	This work
Ni5A-DP	DP	9.6	0.212–0.5	0.9	4:1:15	-	13333 mL/g/h	10.8, 280	96.3, 280	0.00419	This work
Ni5A-IE	IE	7.4	0.212–0.5	0.9	4:1:15	-	13333 mL/g/h	8.5, 280	100, 280	0.00330	This work
5 %Ni13X-EIM−350	EIM	13.5	0.212–0.5	0.9	4:1:15	-	13333 mL/g/h	18.5, 280	53.5, 280	0.00718	[15]
5 %Ni13X-EIM−450	EIM	11.6	0.212–0.5	0.9	4:1:15	-	13333 mL/g/h	14.9, 280	45.3, 280	0.00578	[15]
5 %Ni/MSN	EIM	9.9	0.2–0.4	0.2	4:1:0	200	50000 mL/g/h	82, 350	99.9, 350	0.11960	[46]
5 %NiUSY	IWI	-	-	0.2	36:9:10	-	43000/h	9.4, 300	-	0.02052	[17]
5 %NiUSY	IWI	17–33	-	0.2	36:9:10	10	43000/h	6.7, 300	93.1, 300	0.01463	[19]
5 %NiMSN	WI	9.9	0.02–0.04	0.2	4:1:0	200	50000 mL/g/h	64.1, 300	99.9, 300	0.09349	[22]
5 %Ni/MCM−41	WI	10.5	0.02–0.04	0.2	4:1:0	140	50000 mL/g/h	56.5, 300	98.3, 300	0.08241	[22]
5 %Ni/HY	WI	19.8	0.02–0.04	0.2	4:1:0	140	50000 mL/g/h	48.5, 300	96.4, 300	0.07074	[22]
5 %Ni/SiO_2	WI	17.8	0.02–0.04	0.2	4:1:0	140	50000 mL/g/h	42.4, 300	96.6, 300	0.06184	[22]
5 %Ni/γ-Al_2O_3	WI	-	0.02–0.04	0.2	4:1:0	100	50000 mL/g/h	27.6, 300	95.2, 300	0.04026	[22]
5 %Ni/a-TiO_2	WI	8.7–12.9	0.425–0.85	0.1	19:76:5	-	15000 mL/g/h	58.2, 360	90, 360	0.02541	[47]
5 %Ni/13X	EIM	33	2	250	4.05:1:0	10	92/h	78.8, 300	100, 300	0.00001	[14]
5 %Ni/5 A	EIM	22	2	250	4.05:1:0	10	92/h	78.8, 300	100, 300	0.00001	[14]
Ni−5A	IWI	7.6	0.25–0.60	0.2	4:1:0	-	30000 mL/g/h	10, 300	80, 300	0.00873	[40]
Ni−13X	IWI	6.8	0.25–0.60	0.2	4:1:0	50	30000 mL/g/h	20, 300	56, 300	0.01747	[40]
15Ni/USY	IWI	21	Powder	0.2	6:1:3	8	82200 mL/g/h	20, 300	93, 300	0.01140	[48]
15Ni/NaY	WI	17.89	0.02–0.04	0.2	4:1:0	40	50000 mL/g/h	47, 300	51, 300	0.02285	[49]
15Ni/Cs-USYH2O	IWI	20	Powder	0.2	36:9:10	13	86100 mL/g/h	17, 300	90, 300	0.01420	[50]
6 %Ni/TiO_2	WI	4.6	-	0.05	24:6:10	-	48000 mL/g/h	3, 300	99, 300	0.00349	[51]
5 %Ni/TiO_2-Na	WI	45.8	Powder	0.1	4:1:0	-	24000 mL/g/h	14, 300	40, 300	0.00978	[52]
5 %Ni/TiO_2 NWs	IWI	14.43	Powder	0.3	4:1:0	40	9400 mL/g/h	82, 300	98, 300	0.02244	[53]
5 %Ni/HNTs	WI	15.2	-	0.48	4:1:1	50	15000 mL/g/h	55, 300	93, 300	0.02402	[54]

[a] HY = protonated Y zeolite; USY = ultra-stable Y zeolite; NaY = NaY zeolite; TiO_2 NWs = TiO_2 nanowires; HNTs = Halloysite nanotubes.
[b] Catalyst preparation method, EIM = evaporation impregnation method, DP=deposition precipitation, IE = ion exchange, IWI = incipient wetness impregnation, WI = wet impregnation method.
[c] Active metal cluster size.
[d] Catalyst particle size.
[e] Stability of the catalysts.
[f] Calculated under the specific temperature based on the total Ni metal in catalyst.

zeolite catalyst synthesis in CO_2 methanation.

Funding

This research was funded by the China Scholarship Council (CSC), File No. 201608430104.

CRediT authorship contribution statement

de Jong Wiebren: Writing – review & editing, Supervision, Project administration, Methodology, Funding acquisition, Formal analysis. **Grénman Henrik:** Writing – review & editing, Supervision, Project administration, Methodology, Formal analysis, Conceptualization. **Peurla Markus:** Data curation. **Peltonen Janne:** Data curation. **Haije Wim:** Writing – review & editing, Supervision. **Kumar Narendra:** Writing – review & editing, Validation, Supervision, Formal analysis, Conceptualization. **Wei Liangyuan:** Writing – review & editing, Writing – original draft, Validation, Resources, Methodology, Investigation, Funding acquisition, Formal analysis, Data curation, Conceptualization.

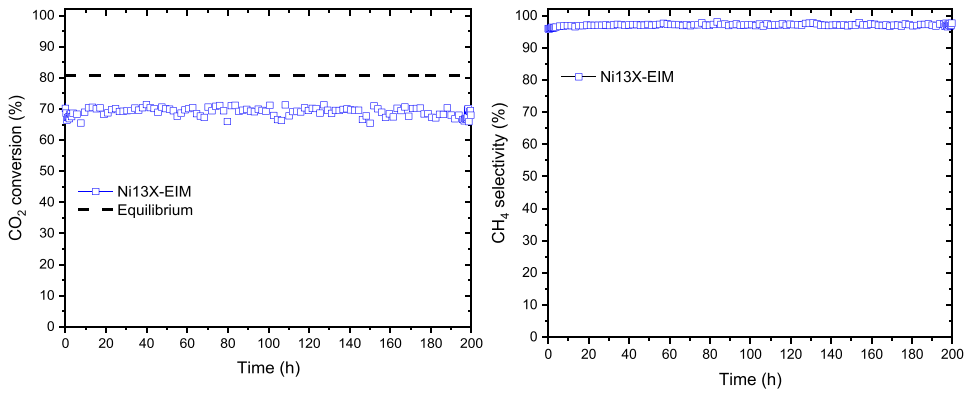

Fig. 7. CO_2 conversion and CH_4 selectivity of stability test at 360 °C for Ni13X-EIM (0.9 g, reduction at 500 °C, 4 h), 150 mL/min N_2, 40 mL/min H_2, 10 mL/min CO_2.

Declaration of Competing Interest

The authors declare the following financial interests/personal relationships which may be considered as potential competing interests: Wiebren de Jong reports financial support was provided by China Scholarship Council. If there are other authors, they declare that they have no known competing financial interests or personal relationships that could have appeared to influence the work reported in this paper

Acknowledgements

The research work is a part of the activities of Process and Energy department in Delft University of Technology and Johan Gadolin Process Chemistry Centre, a centre of excellence financed by Åbo Akademi University. The authors acknowledge the Åbo Akademi University, The Finnish Society of Science and Letters for funding the visiting of Liangyuan at Turku. The authors also acknowledge the PhD scholarship awarded to Liangyuan Wei by the China Scholarship Council.

Appendix A. Supporting information

Supplementary data associated with this article can be found in the online version at doi:10.1016/j.cattod.2025.115239.

Data availability

Data will be made available on request.

References

[1] H. Yang, et al., Progress in carbon dioxide separation and capture: a review, J. Environ. Sci. (China) 20 (1) (2008) 14–27.
[2] Z.A. Manan, et al., Advances in Process Integration research for CO_2 emission reduction–a review, J. Clean. Prod. 167 (2017) 1–13.
[3] M. Bailera, et al., Power to Gas projects review: lab, pilot and demo plants for storing renewable energy and CO_2, Renew. Sustain. Energy Rev. 69 (2017) 292–312.
[4] F.A. Rahman, et al., Pollution to solution: capture and sequestration of carbon dioxide (CO_2) and its utilization as a renewable energy source for a sustainable future, Renew. Sustain. Energy Rev. 71 (2017) 112–126.
[5] V. Sebestyén, Renewable and sustainable energy reviews: environmental impact networks of renewable energy power plants, Renew. Sustain. Energy Rev. 151 (2021) 111626.
[6] T. Schaaf, et al., Methanation of CO_2-storage of renewable energy in a gas distribution system, Energy, Sustain. Soc. 4 (1) (2014) 2.
[7] P. Frontera, et al., Supported catalysts for CO_2 methanation: a review, Catalysts 7 (2) (2017) 59.
[8] B. Li, et al., Influence of addition of a high amount of calcium oxide on the yields of pyrolysis products and noncondensable gas evolving during corn stalk pyrolysis, Energy Fuels 31 (12) (2017) 13705–13712.
[9] B. Li, et al., Effects of different calcium-based absorbents on hydrogen production of corn stalk pyrolysis-gasification, Renew. Energy Resour. 35 (4) (2017) 502–507.
[10] S. Walspurger, et al., Sorption enhanced methanation for substitute natural gas production: Experimental results and thermodynamic considerations, Chem. Eng. J. 242 (2014) 379–386.
[11] V.M. Lebarbier, et al., Sorption-enhanced synthetic natural gas (SNG) production from syngas: a novel process combining CO methanation, water-gas shift, and CO_2 capture, Appl. Catal. B: Environ. 144 (1) (2014) 223–232.
[12] A. Borgschulte, et al., Sorption enhanced CO_2 methanation, Phys. Chem. Chem. Phys. 15 (24) (2013) 9620–9625.
[13] L. Wei, et al., Pure methane from CO_2 hydrogenation using a sorption enhanced process with catalyst/zeolite bifunctional materials, Appl. Catal. B: Environ. 297 (2021) 120399.
[14] R. Delmelle, et al., Development of improved nickel catalysts for sorption enhanced CO_2 methanation, Int. J. Hydrog. Energy 41 (44) (2016) 20185–20191.
[15] L. Wei, et al., Influence of nickel precursors on the properties and performance of Ni impregnated zeolite 5A and 13X catalysts in CO_2 methanation, Catal. Today 362 (2021) 35–46.
[16] L. Wei, et al., Can bi-functional nickel modified 13X and 5A zeolite catalysts for CO_2 methanation be improved by introducing ruthenium? Mol. Catal. 494 (2020) 111115.
[17] A. Westermann, et al., Insight into CO_2 methanation mechanism over NiUSY zeolites: An operando IR study, Appl. Catal. B: Environ. 174-175 (2015) 120–125.
[18] M.C. Bacariza, et al., CO_2 hydrogenation over Ni-based zeolites: effect of catalysts preparation and pre-reduction conditions on methanation performance, Top. Catal. 59 (2-4) (2015) 314–325.
[19] I. Graça, et al., CO_2 hydrogenation into CH_4 on NiHNaUSY zeolites, Appl. Catal. B: Environ. 147 (ement C) (2014) 101–110.
[20] M.A.A. Aziz, et al., CO_2 methanation over heterogeneous catalysts: recent progress and future prospects, Green Chem. 17 (5) (2015) 2647–2663.
[21] S. Rönsch, et al., Review on methanation – from fundamentals to current projects, Fuel 166 (2016) 276–296.
[22] M.A.A. Aziz, et al., Highly active Ni-promoted mesostructured silica nanoparticles for CO_2 methanation, Appl. Catal. B: Environ. 147 (2014) 359–368.
[23] F. Wang, et al., Photocatalytic CO_2 methanation over the Ni/SiO_2 catalysts for performance enhancement, Int. J. Hydrog. Energy 68 (2024) 1382–1392.
[24] J. Gao, et al., Recent advances in methanation catalysts for the production of synthetic natural gas, RSC Adv. 5 (29) (2015) 22759–22776.
[25] A. Westermann, et al., The promoting effect of Ce in the CO_2 methanation performances on NiUSY zeolite: a FTIR In Situ/Operando study, Catal. Today 283 (2017) 74–81.
[26] A. Quindimil, et al., Ni catalysts with La as promoter supported over Y- and BETA-zeolites for CO_2 methanation, Appl. Catal. B: Environ. 238 (2018) 393–403.
[27] L. Wei, et al., Sub-nanometer ceria-promoted Ni 13X zeolite catalyst for CO_2 methanation, Appl. Catal. A: Gen. 612 (2021) 118012.
[28] E. Marceau, et al., Ion Exchange and Impregnation (et al.), in: G. Ertl (Ed.), Handbook of Heterogeneous Catalysis, Wiley-VCH Verlag GmbH & Co. KGaA, 2008, pp. 467–484 (et al.).
[29] G.L. Price, Solid-State Ion-Exchange of Zeolites, in: J. Regalbuto (Ed.), Catalyst preparation: science and engineering, CRC Press: Boca Raton, 2006, pp. 283–295.
[30] C. Louis, Deposition-precipitation synthesis of supported metal catalysts, in: J. Regalbuto (Ed.), in Catalyst Preparation: Science and Engineering, CRC Press: Boca Raton, 2006, pp. 319–339.
[31] P. Sheena, et al., Effect of calcination temperature on the structural and optical properties of nickel oxide nanoparticles, Nanosyst.: Phys., Chem., Math. 3 (5) (2014) 441–449.
[32] J. Estellé, et al., Comparative study of the morphology and surface properties of nickel oxide prepared from different precursors, Solid State Ion. 156 (1) (2003) 233–243.
[33] Odenberger, M., *Integration of power-to-gas in gasendal and gobigas*, in *Energy and Environment*. 2013, CHALMERS UNIVERSITY OF TECHNOLOGY: Göteborg, Sweden.
[34] H. Qiao, et al., Preparation and characterization of NiO nanoparticles by anodic arc plasma method, J. Nanomater. 2009 (1) (2009) 795928.

[35] J.M. Adams, D.A. Haselden, The structure of dehydrated zeolite 5A (.) by neutron profile refinement, J. Solid State Chem. 51 (1) (1984) 83–90.
[36] X.F. Yang, et al., Single-atom catalysts: a new frontier in heterogeneous catalysis, Acc. Chem. Res 46 (8) (2013) 1740–1748.
[37] B.H. Chen, et al., Towards a full understanding of the nature of Ni(II) species and hydroxyl groups over highly siliceous HZSM-5 zeolite supported nickel catalysts prepared by a deposition-precipitation method, Dalton Trans. 45 (6) (2016) 2720–2739.
[38] P. Burattin, M. Che, C. Louis, Molecular approach to the mechanism of deposition−precipitation of the Ni (II) phase on silica, J. Phys. Chem. B 102 (15) (1998) 2722–2732.
[39] R. Nares, et al., Ni/Hβ-zeolite catalysts prepared by deposition−precipitation, J. Phys. Chem. B 106 (51) (2002) 13287–13293.
[40] P. Yan, et al., Impact of varied zeolite materials on nickel catalysts in CO_2 methanation, J. Catal. 432 (2024) 115439.
[41] M. Boronat, A. Corma, What is measured when measuring acidity in zeolites with probe molecules? ACS Catal. 9 (2) (2019) 1539–1548.
[42] D. Jin, et al., Microwave assisted in situ synthesis of USY-encapsulated heteropoly acid (HPW-USY) catalysts, Appl. Catal. A: Gen. 352 (1-2) (2009) 259–264.
[43] F. Arena, R. Dario, A. Parmaliana, A characterization study of the surface acidity of solid catalysts by temperature programmed methods, Appl. Catal. A: Gen. 170 (1) (1998) 127–137.
[44] F. Lónyi, J. Valyon, On the interpretation of the NH_3-TPD patterns of H-ZSM-5 and H-mordenite, Microporous Mesoporous Mater. 47 (2) (2001) 293–301.
[45] S. Abate, et al., Synthesis, characterization, and activity pattern of Ni–Al hydrotalcite catalysts in CO_2 methanation, Ind. Eng. Chem. Res. 55 (30) (2016) 8299–8308.
[46] M.A.A. Aziz, et al., CO_2 methanation over Ni-promoted mesostructured silica nanoparticles: Influence of Ni loading and water vapor on activity and response surface methodology studies, Chem. Eng. J. 260 (2015) 757–764.
[47] J. Li, et al., Enhanced CO_2 methanation activity of Ni/anatase catalyst by tuning strong metal–support interactions, ACS Catal. 9 (7) (2019) 6342–6348.
[48] D. Spataru, et al., Doping Ni/USY zeolite catalysts with transition metals for CO_2 methanation, Int. J. Hydrog. Energy 53 (2024) 468–481.
[49] N.A. Sholeha, et al., Enhanced CO_2 methanation at mild temperature on Ni/zeolite from kaolin: effect of metal–support interface, RSC Adv. 11 (27) (2021) 16376–16387.
[50] M.C. Bacariza, et al., Boosting Ni dispersion on zeolite-supported catalysts for CO_2 methanation: the influence of the impregnation solvent, Energy Fuels 34 (11) (2020) 14656–14666.
[51] P. Unwiset, et al., Catalytic activities of titania-supported nickel for carbon-dioxide methanation, Chem. Eng. Sci. 228 (2020) 115955.
[52] R. Pérez-Hernández, et al., Carbon cycle using the CO_2 conversion to methane as environmental feasibility on Ni/TiO_2-Na nanotubes catalysts, Renew. Energy 217 (2023) 119145.
[53] W.K. Fan, et al., Catalytic CO_2 hydrogenation to produce methane over NiO/TiO_2 composite: effect of TiO_2 structure, Int. J. Hydrog. Energy 51 (2024) 462–478.
[54] D. Yang, et al., Enhanced CO_2 Methanation over Ni/Na-HNTs: effect of Pretreatment with NaOH, Ind. Eng. Chem. Res. 63 (14) (2024) 6469–6479.
[55] S. Tada, et al., Effect of Ru and Ni ratio on selective CO methanation over Ru–Ni/TiO_2, Fuel 129 (2014) 219–224.